Journal of Medicinal Chemistry

pubs.acs.org/jmc Article

Synthesis and Characterization of the Novel Rodent-Active and CNS-Penetrant P2X7 Receptor Antagonist Lu AF27139

Allen T. Hopper,* Martin Juhl, Jorrit Hornberg, Lassina Badolo, John Paul Kilburn, Annemette Thougaard, Gennady Smagin, Dekun Song, Londye Calice, Veena Menon, Elena Dale, Hong Zhang, Manuel Cajina, Megan E. Nattini, Adarsh Gandhi, Michel Grenon, Ken Jones, Tanzilya Khayrullina, Gamini Chandrasena, Christian Thomsen, Stevin H. Zorn, Robb Brodbeck, Suresh Babu Poda, Roland Staal, and Thomas Möller

Cite This: *J. Med. Chem.* 2021, 64, 4891−4902 Read Online

ACCESS | Metrics & More | Article Recommendations | Supporting Information

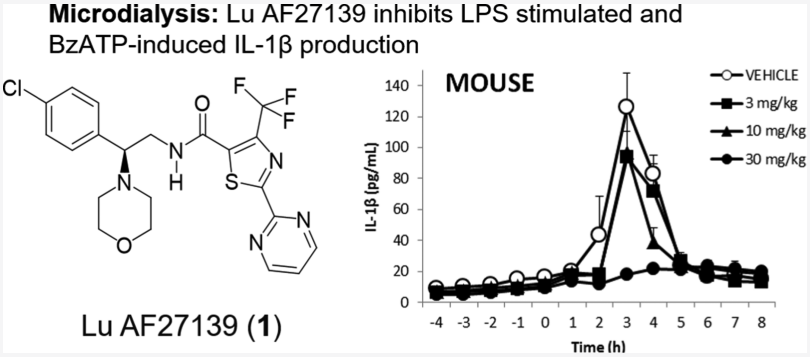

ABSTRACT: There remains an insufficient number of P2X7 receptor antagonists with adequate rodent potency, CNS permeability, and pharmacokinetic properties from which to evaluate CNS disease hypotheses preclinically. Herein, we describe the molecular pharmacology, safety, pharmacokinetics, and functional CNS target engagement of Lu AF27139, a novel rodent-active and CNS-penetrant P2X7 receptor antagonist. Lu AF27139 is highly selective and potent against rat, mouse, and human forms of the receptors. The rat pharmacokinetic profile is favorable with high oral bioavailability, modest clearance (0.79 L/(h kg)), and good CNS permeability. *In vivo* mouse CNS microdialysis studies of lipopolysaccharide (LPS)-primed and 2′(3′)-*O*-(benzoylbenzoyl)-adenosine-5′-triphosphate (BzATP)-induced IL-1β release demonstrate functional CNS target engagement. Importantly, Lu AF27139 was without effect in standard *in vitro* and *in vivo* toxicity studies. Based on these properties, we believe Lu AF27139 will be a valuable tool for probing the role of the P2X7 receptor in rodent models of CNS diseases.

INTRODUCTION

The P2X7 receptor (P2X7R) is an adenosine triphosphate (ATP) gated nonselective cation channel with a relatively high km for ATP in the 100−1000 μM range *in vitro*.[1] Existing as a homotrimer, P2X7Rs are widely expressed throughout the CNS including the spinal cord with cellular localization predominantly on microglia.[2] Peripherally, P2X7R is expressed on immune cells (e.g., monocytes, neutrophils, T, B, NK cells), Schwann cells, and satellite glia. Activation of the P2X7R ion channel by ATP leads to immediate calcium influx and a variety of associated downstream signaling events, including triggering the maturation and release of the cytokines IL-1β and IL-18.[3]

Owing to its localization on microglia and importance in regulating inflammatory cytokines, P2X7R has been suggested to play an important role in neuroinflammation[4] and has been implicated in a variety of CNS-based diseases[5−8] including neuropathic pain (NPP),[9] multiple sclerosis (MS), Alzheimer's disease (AD), epilepsy, Huntington's disease, and major depressive disorder (MDD).[10,11] While significant progress has been made in the identification of human selective P2X7 antagonists, at the start of this work, there remained an insufficient number of CNS-permeable P2X7 receptor antagonist tools from which to probe rodent CNS pharmacology.[12] Significant cross-species differences in molecular pharmacology and insufficient CNS permeability hampered the use of many P2X7 receptor antagonists for this purpose.[13]

Received: December 28, 2020
Published: April 6, 2021

https://doi.org/10.1021/acs.jmedchem.0c02249
J. Med. Chem. 2021, 64, 4891−4902

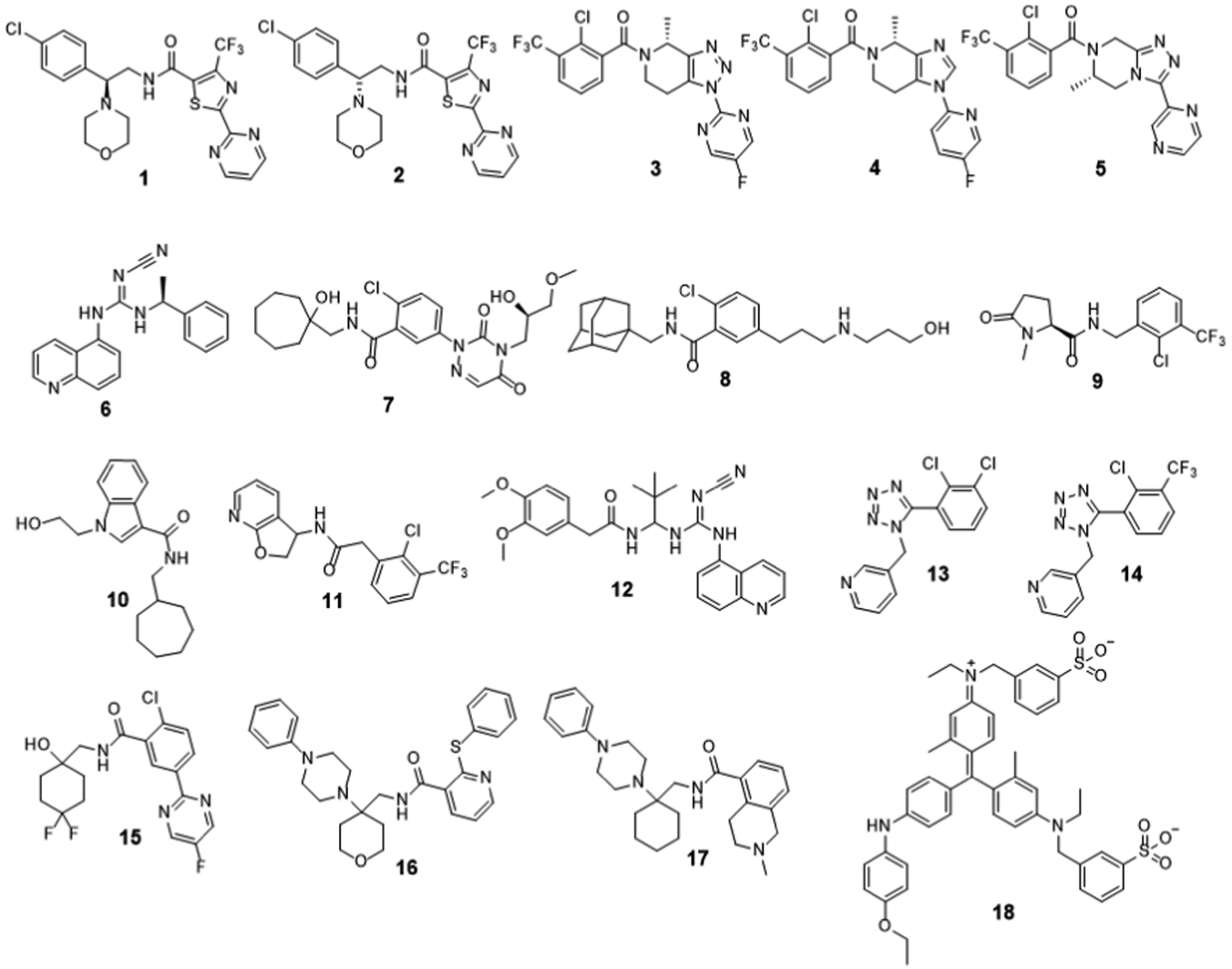

Figure 1. Chemical structures of Lu AF27139 (**1**), Lu AF27138 (**2**), and P2X7R comparator compounds JNJ-54175446 (**3**), JNJ-54166060 (**4**), JNJ analogue (**5**), A-804598 (**6**), CE224,535 (**7**), AZD9056 (**8**), GSK1482160 (**9**), AFC5128 (**10**), Actelion compound (**11**), A-740003 (**12**), A-438079 (**13**), Abbott compound (**14**), Pfizer compound (**15**), JNJ-47965567 (**16**), JNJ-42253432 (**17**), and BBG (**18**).

Lacking were a sufficient number of structurally distinct tools with optimized pharmacokinetic (PK) and safety profiles, to establish the role of the P2X7R in models where chronic dosing paradigms and near-complete target engagement would be required to adequately test biological hypotheses. Herein, we report the structure, synthesis, molecular pharmacology, ADMET, and safety data for Lu AF27139 (**1**), a rodent-active CNS-penetrant and highly selective P2X7R antagonist.

As part of our drug discovery research related to neuroinflammation, we desired to probe the role of the P2X7R in a variety of CNS disease models (e.g., major depressive disorder, epilepsy, multiple sclerosis, and neuropathic pain). In this vein, we required suitable CNS-penetrant P2X7R antagonist tools capable of giving near-complete functional inhibition of the ion channel under a subchronic dosing paradigm. We evaluated a variety of literature-reported compounds and found them to be generally inadequate for this purpose, as they either lacked sufficient rodent P2X7R potency, did not appreciably enter the CNS, were of poor metabolic stability, or lacked appropriate target selectivity. Therefore, part of our medicinal chemistry work focused on identifying compounds with appropriate characteristics to probe in preclinical rodent models of neuroinflammation and CNS disease. To bolster this effort, the Neurogen P2X7R patent estate was licensed by Lundbeck. The racemic form of compound **1** was previously reported as having an IC_{50} < 2 μM.[14] While we synthesized and tested numerous compounds within and near those within the Neurogen patent estate, racemic **1** stood out as having good potency and properties consistent with good CNS permeability and PK, leading to the desire to separate the two enantiomers giving **1** and **2**.[15]

Subsequent to the conclusion of this work, several valuable CNS-penetrant rodent-active tool compounds were described.[16] The clinical candidate JNJ-54175446 (**3**), with a tetrahydro-triazolopyridine core, was reported to have near-equal rat and human P2X7R potencies with pIC_{50}'s of 8.8 and 8.5, respectively, and a brain-to-plasma ratio of 1.1 ($K_{p,uu,brain}$ 0.46).[17] A similar tetrahydro-imidazolopyridine analogue, JNJ-54166060 (**4**), has rat and human P2X7R pIC_{50}'s of 8.4 and 6.9, respectively, and a $K_{p,uu,brain}$ of 0.84.[13] In addition, a series of CNS-penetrant and rat-active 1,2,4-triazolopiperidines were described, as exemplified by **5**.[18] Compound **5** has rat and human P2X7R pIC_{50}'s of 7.10 and 9.15. Further, **5** has good CNS permeability, as demonstrated by its activity in an *ex vivo*

https://doi.org/10.1021/acs.jmedchem.0c02249
J. Med. Chem. 2021, 64, 4891−4902

Table 1. P2X7 Receptor *In Vitro* Molecular Pharmacology, Metabolic Stability, and Permeability Data

	P2X7 FLIPR data IC_{50} (nM)[a]			P2X7 binding Ki (nM)[b]			IL-1β IC_{50} (nM)[c]	liver microsomal stability (L/(h kg))[d]		MDCK-1 Papp (cm/s × 10^{-6})[e]	
compound	human	rat	mouse	human	rat	mouse	human	human	rat	A:B	ER
1	12 ± 0.52	2.4 ± 0.094	22 ± 1.2	55 ± 9.8	13 ± 2.4	180 ± 71	38 ± 2.5	2.6	5.1	15	0.81
2	90 ± 6.5	95 ± 6.2									
6	32 ± 4.1	6.1 ± 0.60	34 ± 2.8	8.9 ± 0.61	3.9 ± 0.36	60 ± 17	15 ± 5.7	1.4	4.3	9.3	1.5
7	0.76 ±0.08	470 ± 57	660 ± 69				1.5	1.2	7.2	0.6	27
8	3.5 ±0.75	4.4 ± 1.1	1700 ±340	15 ± 1.9	130 ± 22		1.4	1.2	2.6	0.7	17
9	20 ±1.8	1900 ± 440	2300 ±450	5.7 ± 1.8	510 ± 12		300	0.3	1.0	20	0.72
10	72 ±19	1500 ± 230	240 ± 21					5.3	32	5.9	0.7
11	5.5 ±0.81	260 ± 19	320 ± 53	5.6 ± 1.2		100 ± 28	27 ± 9.0	1.6	5.1	25	0.83
12	81 ±5.5	4.0 ± 0.20	250 ± 75	130 ± 21	59 ± 1.9		290			0.2	66
13	2100 ±390	910 ± 160	2900 ±490	68 ± 37	200 ± 42		150	1.0	46		
14	57 ±15	71 ± 6.9	300 ± 35	7.4 ± 1.6	16 ± 2.0	48 ± 13	140 ± 16	4.5	25	40	0.77
15	21 ±1.5	5500 ± 1300	>10 000	53 ± 3.0	4800 ± 63			0.47	3.2	18	0.6
16	35 ±2.3	4.7 ± 0.82	0.65 ± 0.12		98			17	26	11	1.1
17									12	0.25	1.1
18	5800 ±1700	200 ± 63	1300 ± 65	>10 000	1000 ± 36		700				

[a]P2X7R FLIPR data were determined in HEK293 cells stably transfected with either human, rat, or mouse P2X7R. The cells were preincubated with antagonist and then stimulated with an EC_{80} concentration of BzATP. [b]P2X7R binding was performed in membranes prepared from the same cells using [^{3}H]-A-804598 as the radio-ligand. Values are expressed as mean ± standard error of the mean (SEM) for $n \geq 3$ experiments. [c]IL-1β inhibition data in THP-1 cells primed with lipopolysaccharide (LPS) and stimulated with BzATP. [d]Rat and human liver microsomal intrinsic clearance (Clint) was determined by assessing the disappearance of test compounds at six time points over a 60 min incubation period. The compounds (1 μM) were incubated in a 1 mL reaction volume containing rat or human liver microsomes (purchased from Becton Dickinson, MA) at a concentration of 0.7−1.0 mg protein/mL and fortified with NADPH. [e]MDR1-MDCK cell permeability of the test compounds from A to B direction or B to A direction was determined in triplicate, and the efflux ratio (ER) is the ratio of B:A/A:B permeation. Experimental details are described in the Supporting Information.

receptor occupancy assay in rat hippocampus with an ED_{50} of 0.8 mg/kg. Compound **1** adds structural diversity to the growing list of tool P2X7R inhibitors of potential utility to probe in preclinical rodent models of neuroinflammation and CNS diseases.

RESULTS AND DISCUSSION

Compound **1**,[15] its enantiomer Lu AF27138 (**2**) and comparator P2X7R antagonists A-804598 (**6**),[19] CE224,535 (**7**),[20] AZD9056 (**8**),[21] GSK1482160 (**9**),[22,23] AFC5128 (**10**),[24] Actelion compound (**11**),[25] A-740003 (**12**),[26] A-438079 (**13**),[27] Abbott compound (**14**),[28] Pfizer compound (**15**),[29] JNJ-47965567 (**16**),[30] JNJ-42253432 (**17**),[31] and BBG (**18**)[32] were tested *in vitro* against mouse, rat, and human forms of the receptor for inhibiting 2′(3′)-*O*-(benzoylbenzoyl)adenosine-5′-triphosphate (BzATP)-induced calcium-flux using fluorescent imaging plate reader (FLIPR)-based assays (Figure 1 and Table 1). While ATP is the endogenous agonist for the P2X7 receptor, BzATP is a more stable, potent, and selective agonist of the P2X7 receptor and therefore commonly used to activate the receptor in a variety of assays.[33] Compound **1** was found to have similar P2X7R potency against rat (IC_{50} 2.2 nM, Ki 13 nM), mouse (IC_{50} 22 nM, Ki 180 nM), and human (IC_{50} 12 nM, Ki 38 nM) forms of the receptors. Since *S*-enantiomer **1** was 7.5- and 40-fold more potent against human and rat forms of the receptor, respectively, than *R*-enantiomer **2**, additional work focused only on enantiomer **1**. Binding experiments were performed in cell membranes isolated from HEK293 cells stably transfected with human, rat, or mouse P2X7R. Compound **1** was about 5-fold less potent in the binding assays than in the functional FLIPR assays. While many of the reference compounds have similarly low nanomolar potency against human P2X7R, compounds **7**, **9**, **10**, **11**, and **15**, are from 100- to 1000-fold less potent at the rodent receptor, thus limiting their usefulness to probe rodent *in vivo* pharmacology. Potency shifts between mouse and rat P2X7R were also observed, such as for **8** and **12** with 390- and 60-fold shifts in potency between rodent species, respectively. Notable differences between the measured binding Ki and FLIPR IC_{50}'s for some compounds may reflect differences in on and off rates. For example, **1** and **8** are 5- and 30-fold more potent in the rat FLIPR assay than rat binding Ki, respectively, while **13** and **14** have rat binding Ki's 4.5- and 4.4-fold more potent than their respective rat FLIPR IC_{50}'s. These compounds were also evaluated for their ability to inhibit IL-1β release in THP-1 cells, a human cell line. With a few exceptions, the IC_{50} for inhibiting IL-1β release was within 3-fold of the human P2X7 FLIPR data IC_{50}'s. Compound **1** was 3-fold less potent at inhibiting IL-1β release in THP-1 cells with an IC_{50} of 38 nM, than inhibiting Ca^{++} flux in the human P2X7 FLIPR assay. A few compounds, such as **6**, **8**, **13**, and **18**, were more potent at inhibiting IL-1β release than in the human FLIPR assay. Despite these differences, a reasonable correlation between the two assays was observed.

Beyond species selectivity, ADME properties associated with low brain permeability and high intrinsic clearance have ultimately led to insufficient exposure for hypothesis testing with many P2X7R antagonists. Liver microsomal stability and permeability in the MDR1-MDCK cell assay were evaluated for representative tools (Table 1). Compounds **10**, **13**, **14**, **16**, and **17** have particularly high rates of intrinsic clearance measured in rat liver microsomes at 4- to 10-fold above rat hepatic blood flow. Metabolic instability is undesirable as it may preclude from running subchronic dosing studies and could produce large amounts of interfering metabolites, thus complicating interpretation of *in vivo* efficacy studies. The

https://doi.org/10.1021/acs.jmedchem.0c02249
J. Med. Chem. 2021, 64, 4891−4902

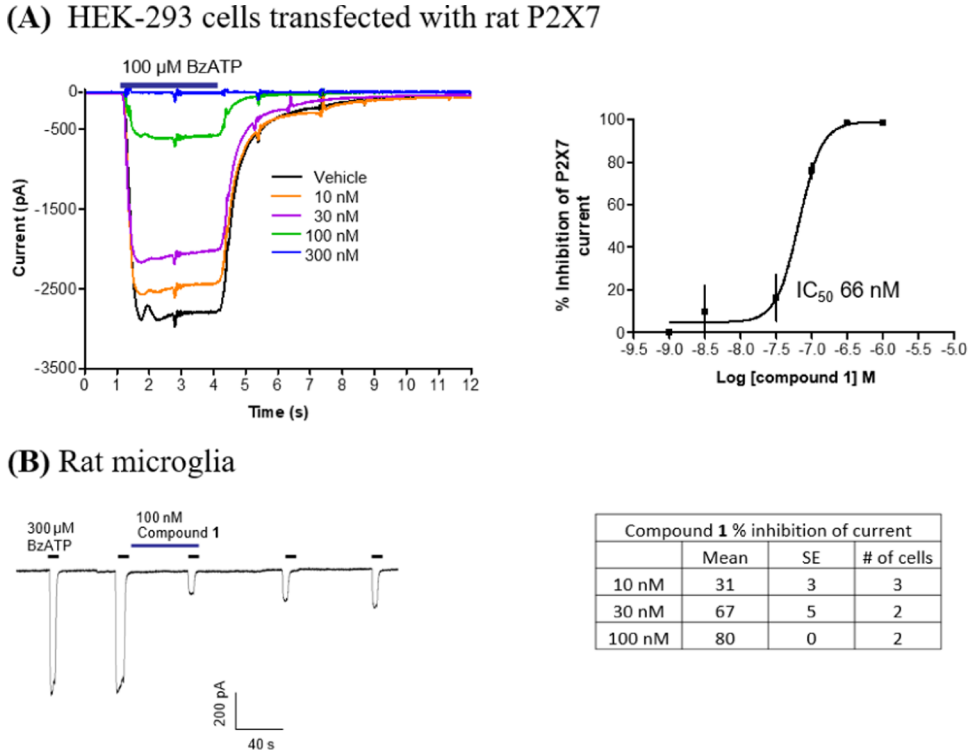

Compound **1** % inhibition of current			
	Mean	SE	# of cells
10 nM	31	3	3
30 nM	67	5	2
100 nM	80	0	2

Figure 2. Compound **1** inhibits BzATP-induced currents in (A) HEK293 cells stably transfected with rat P2X7R and (B) rat primary microglia. Repeated administration of 300 μM BzATP demonstrates a slowly reversible effect of a single 60 s administration of 100 nM **1**.

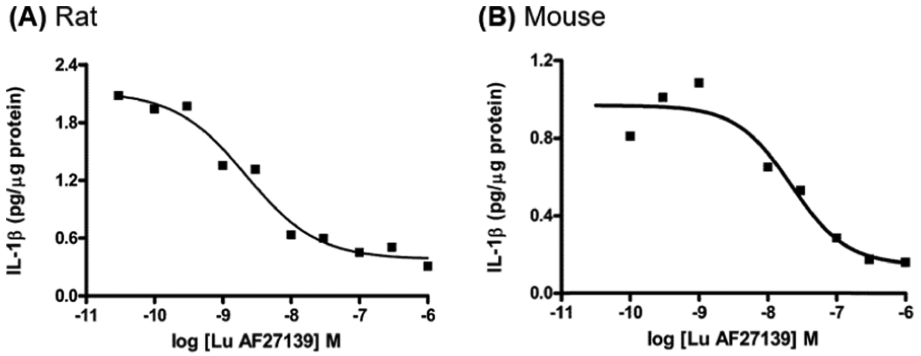

Figure 3. Compound **1** concentration-dependently inhibits IL-1β release in rat and mouse primary cortical microglia primed with LPS and induced with 1 mM BzATP (A) rat microglia IL-1β release with an average IC_{50} of 38 ± 19 nM (n = 4). The rat IC_{50} of the example curve is 2.2 nM, and (B) mouse IL-1β release with an IC_{50} of 26 ± 6 nM (n = 3). The mouse IC_{50} for the example curve is 21.9 nM.

MDR1-MDCK cell permeability assay is a useful predictor of CNS permeability and Pgp efflux liabilities. Compounds **7**, **8**, **12**, and **17** have low permeability with apical to basolateral permeation being less than 1.0×10^{-6} cm/s with varying efflux ratios, defined as the rate going from basolateral to apical divided by the rate moving from apical to basolateral direction. However, compounds **1**, **9**, **11**, **14**, **15**, and **16** have desired moderate to high permeability with Pgp efflux ratios below 2.

P2X7R antagonist **6** appeared to be an excellent tool compound candidate owing to its good rodent potency, permeability, and metabolic stability properties. However, possibly due to its low solubility, a formulation and dosing paradigm to give sufficient and reproducible exposures could not be identified, despite considerable efforts to do so (unpublished data). During our discovery efforts, the novel compound **1** was found to have similar P2X7R potency to rat (IC_{50} 2.2 nM, Ki 13 nM), mouse (IC_{50} 22 nM, Ki 180 nM), and human (IC_{50} 12 nM, Ki 38 nM) forms of the receptors. And compound **1** with high permeability in the MDR1-MDCK assay without efflux and suitable metabolic stability became a compound of interest for additional profiling.

To evaluate the effects of **1** on the P2X7R ion channel, it was profiled in several additional P2X7R functional cell-based assays. In electrophysiology experiments, **1** inhibited 100 μM BzATP-induced current in HEK293 cells stably transfected with the rat P2X7R (Figure 2A) in a dose response manner with an IC_{50} of 66 nM. Similarly, **1** inhibited 300 μM BzATP-induced current in primary rat microglia (Figure 2B) with 80% inhibition occurring at a 100 nM dose. This experimental paradigm reveals a slow off-rate of the compound, as it took 17.6 min to regain 50% of the normal response to repeated application of 300 μM BzATP. This can be observed in Figure 2B, where the first two repeat applications of 300 μM BzATP are administered after repeated 80 s of washout with a slow

https://doi.org/10.1021/acs.jmedchem.0c02249
J. Med. Chem. 2021, 64, 4891−4902

Table 2. Exposure of Lu AF27139 (1) in Rat after Oral Administration

dose	$C_{u,\,plasma}$ (nM)[a]		$C_{u,\,brain}$ (nM)[a]		$C_{u,\,spinal\ cord}$ (nM)[a]	
(mg/kg, po)	(1 h)	(2 h)	(1 h)	(2 h)	(1 h)	(2 h)
1	22.4 ± 4.2	22.8 ± 10	5.4 ± 2.6	6.4 ± 2.0	5.20 ± 0.80	10.0 ± 2.0
3	71.2 ± 14	91.4 ± 20	42.2 ± 4.6	30.4 ± 9.4	33.0 ± 3.8	38.2 ± 9.6
10	381 ± 97	164 ± 63	89.6 ± 16	94.2 ± 53	106 ± 19	96.8 ± 22
30	414 ± 100	556 ± 67	272 ± 53	436 ± 61	283 ± 100	293 ± 130
100	1460 ± 240	497 ± 140	1120 ± 180	743 ± 110	705 ± 87	647 ± 110

[a]Free plasma, brain, and spinal cord concentrations of Lu AF27139 in rat were determined by the formula ($Ct*f_u$), where Ct is the total tissue (plasma, brain, or spinal cord) drug concentration and f_u is the fraction unbound in these tissues as determined by *ex vivo* equilibrium dialysis. Values are expressed as mean ± SEM for $n = 3$ animals. $f_{u,\,plasma} = 0.02 \pm 0.00$, $f_{u,\,spinal\ cord} = 0.07 \pm 0.03$, and $f_{u,\,brain} = 0.09 \pm 0.03$. Values are expressed as mean ± SEM for $n \geq 3$ experiments.

rate of current recovery. The difference in potency for **1** between the rat FLIPR assay (IC_{50} 2.3 nM) and the electrophysiology experiments may be due to the different levels of BzATP used. The rat FLIPR assay was run by stimulating cells with an EC_{80} of BzATP (c.a. ∼ 4 μM), which is 25- to 75-fold below that used in the electrophysiology experiments. Data from the electrophysiology assays along with that from the binding assay (rat Ki 13 nM) confirm that **1** antagonizes P2X7R through direct receptor interaction. The finding that **1** is effective in primary rat microglia confirms the presence of functional P2X7R on microglia.

Beyond its ion channel function, P2X7R activation has long been known to regulate IL-1β.[3] IL-1β is carefully regulated *in vivo*, and its production requires two steps: a priming step via activation of the TLR4 receptor to generate pro-IL-1β and subsequent activation of the P2X7R with ATP or the agonist BzATP, thereby triggering inflammasome assembly and activation of caspase 1, which cleaves pro-IL-1β to give mature active IL-1β.[34] Consistent with being a P2X7R antagonist, **1** inhibits LPS-primed and BzATP-induced IL-1β release from THP-1 cells with an IC_{50} of 38 ± 2.5 nM. Similarly, P2X7R antagonist **1** concentration-dependently blocked IL-1β release in rat and mouse primary cortical microglia primed with LPS and induced with 1 mM BzATP with IC_{50}'s of 38 ± 19 nM in rat and 26 ± 6 nM in mice (Figure 3).

The cross-reactivity of **1** was evaluated at a 10 μM concentration against a combination of 84 binding, cellular, and nuclear receptor functional and enzyme assays at CEREP and in the KINOMEscan screen against 468 kinases at DiscoveRx. In the CEREP screen, a minor signal from the A2A binding assay (34% inhibition of agonist binding) was followed up, but no agonistic or antagonistic activity could be detected. In the KINOMEscan, five kinases were inhibited by 65−90% relative to controls in the initial screen, but these hits were not confirmed upon retesting, suggesting that the initial findings were false-positives. Compound **1** was also clean when tested (n = 4) against the available P2X and P2Y receptors at Axxam. Testing was performed in both agonist and antagonist modes in an eight-point dose response starting at a top dose of 10 μM against hP2RX1, hP2RX2, hP2RX3, hP2RX2/3, hP2RX4, rat P2RX4, hP2RY1, hP2RY2, hP2RY6, hP2RY11, hP2RY12, and hP2RY13. In summary, **1** was without significant effect against the targets tested. The likelihood of off-target activity contributing to the pharmacology of **1** is low based on its selectivity profile.

Compound **1** was further characterized in a variety of physical−chemical and ADME assays. Thermodynamic solubility is 16 μg/mL (32 μM), measured using the shake flask high-performance liquid chromatography (HPLC) method. The TPSA is 80, *c* log *P* is 2.2 (determined by Daylight software version 2.2), and the measured log D is 3.3. Intrinsic clearances for **1** in rat and human liver microsomes are 5.1 and 2.6 L/(h kg) (Table 1), and in rat and human hepatocytes are 4.8 and 0.85 L/(kg h), respectively. Compound **1** does not inhibit CYP3A4, 1A2, 2C9, 2C19, 2D6, 2B6, or 2C8 at up to 25 μM, nor is there a time-dependent inhibition against these cyps at a similar concentration based on a high-throughput assay developed for a parallel measure of both reversible and time-dependent inhibition. However, compound **1** does have mild to moderate CYP3A4 induction potential at 10 μM, as measured in human hepatocytes with a relative increase of 26.9% in CYP3A4 mRNA. This is comparable to levels obtained with the clinically relevant CYP3A inducer, rifampin, at a concentration of 10 μM.

The rat pharmacokinetics of plasma concentration−time profile of **1** following intravenous (iv) (1 mg/kg) and per os (po) (2 mg/kg) administration was characterized by a noncompartment model. The modeling parameter estimates show a low plasma clearance (Cl) of 0.79 L/(h kg) and a moderate volume of distribution at a steady state (V_{ss}) of 0.95 L/kg, resulting in a modest terminal half-life ($T_{1/2}$) of 2.7 h. Following oral administration, **1** was rapidly absorbed (T_{max} = 0.58 h) with a high C_{max} (2.7 μM) and high absolute oral bioavailability ($F\% \geq 100$).

Compound **1** is considered to have desirable physical−chemical and DMPK properties supportive of good oral bioavailability and CNS permeability. Two issues however, high liver microsomal clearance and mild to moderate CYP3A4 induction potential, were identified. Concerns related to the rate of rat liver microsomal clearance (1.5-fold rat liver blood flow, LBF) are tempered owing to the observed low rate of *in vivo* plasma clearance of 0.79 L/(h kg) (0.25-fold rat LBF) and high oral bioavailability in rat.

Exposure assessment was performed in rat (Table 2), and drug concentrations were measured in plasma, brain, and spinal cord at 1 and 2 h after oral administration of **1** at 1, 3, 10, 30, and 100 mg/kg. Exposure was dose-proportional, achieving greater than 700 nM free drug levels in the CNS 1 h and 2 h after a 100 mg/kg, po dose. Based on unbound drug concentrations (C_u), the brain-to-plasma ratio varied from about 25% at 1 mg/kg to near 75% at 30 and 100 mg/kg doses. It remains unclear if the observed differences in B/P ratios across doses are due to efflux mechanisms only apparent at low concentrations. Drug concentrations did not vary between 1 and 2 h post-dose nor did they vary between brain and spinal cord tissue. Importantly, the $C_{u,brain}$ and $C_{u,spinal\ cord}$ values were reasonably dose-proportional. Unbound concentrations of **1** are presented for better comparisons of drug exposure across

https://doi.org/10.1021/acs.jmedchem.0c02249
J. Med. Chem. 2021, 64, 4891−4902

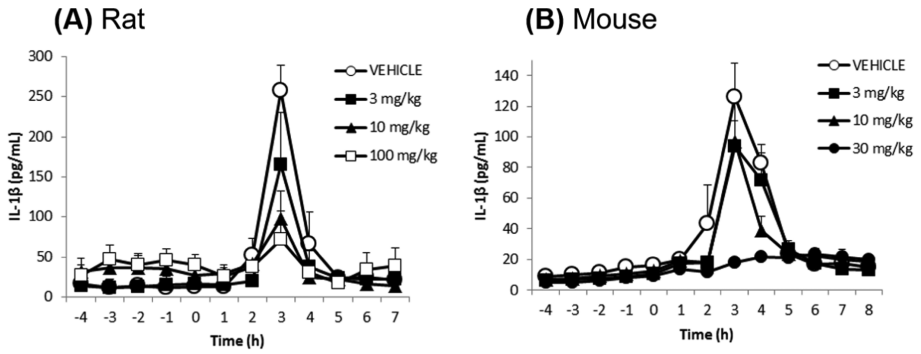

Figure 4. Oral administration of **1** inhibits icv administered LPS-primed and icv BzATP-stimulated IL-1β production in (A) rat and (B) mouse cortex. LPS was administered at time 1 h, compound **1** at time 0, and BzATP at time 1 h. Microdialysis samples were collected every 60 min and IL-1β in the microdialysate samples analyzed using a V-PLEX assay from MesoScale Discovery (Rockville, MD), n = 6 or 7 per time-point. The lower limit of detection was 2 pg/mL for IL-1β. Graphical and statistical analyses performed using GraphPad Prism software (version 5.01). Area under the curve (AUC) was calculated from baseline for each animal between time 0 and 5 h. Analysis of variance (ANOVA) with Dunnett's multiple comparison test was used to determine the significance between treatment groups.

Scheme 1. Synthesis of Lu AF27139 (1); Reagents and Conditions: (a) (i) Morpholine, Tetrahydrofuran (THF); (ii) 2M HCl in Ether; (b) Zn, HCl, EtoH, 87% Crude Yield, Two Steps; (c) *N*-Acetyl-L-leucine, MeCN/H_2O (30:1), 30% Yield, 97% ee; (d) 20, 2,4,6-Tripropyl-1,3,5,2,4,6-trioxatriphosphinane-2,4,6-trioxide (T3P), Triethanolamine (TEA), THF, Room Temperature (RT), 3 h, 62% Yield

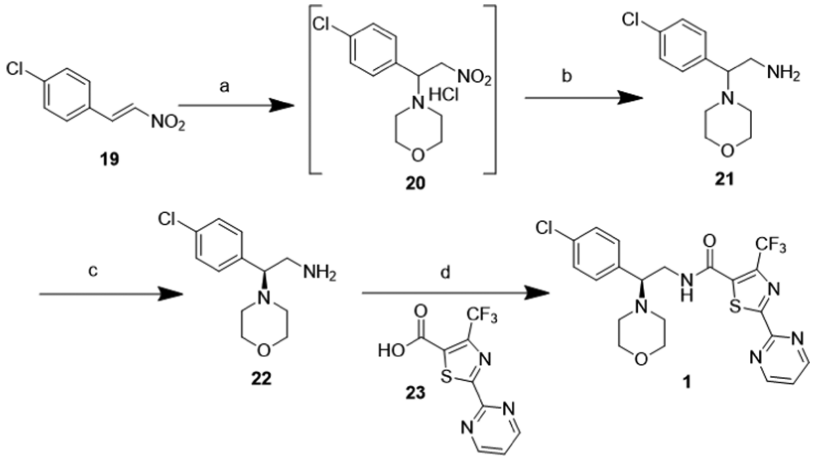

matrices and in line with the free-drug hypothesis where only the unbound concentration of drug is available to bind to the target. Since nonspecific binding of compounds varies in different tissues, ratios such as the brain-to-plasma ratio of drug should be based on the unbound concentrations.[35] Fraction unbound (f_u) of **1** was determined *ex vivo* for rat plasma, brain, and spinal cord tissues utilizing an equilibrium dialysis method (see the Supporting Information). The f_u's in plasma, brain, and spinal cord for **1** are 0.02, 0.09, and 0.07, respectively.

In vivo CNS functional activity was evaluated by measuring IL-1β in the frontal cortex (FC) of freely moving rats and mice using microdialysis (Figure 4). Orally administered **1** reduced intracerebroventricular (icv) administered LPS-primed and BzATP-triggered IL-1β release in the frontal cortex of rats and mice. In contrast to other reports,[30] we did not observe any IL-1β release without LPS priming (data not shown). This is most likely due to the use of low endotoxin human serum albumin (HSA) in the microdialysis perfusion medium. Other investigators report the use of bovine serum albumin (BSA), which is frequently contaminated with endotoxin.[36] Compound **1** was dosed orally 1 h prior to icv BzATP administration and produced minimal effective doses of 3 mg/kg and 10 mg/kg in rats and mice, respectively.

As part of a strategy to identify and mitigate potential safety issues as early as possible during the drug discovery process, **1** was characterized in an exploratory toxicology screening battery.[37] In high content screening and oxidative stress assays, which identify roughly 50% of idiosyncratic hepatotoxic drugs,[38] **1** did not test positive for any of the parameters, including mitochondrial membrane potential, cell count, cell membrane integrity, lysosomal activity, and ROS formation when tested in a dose response manner up to 100 μM. There were no signs of genotoxicity in the miniaturized Ames,[39] *in vitro* micronucleus,[40] and GreenScreen[41] assays. At 30 μM, **1** showed 44% inhibition of the hERG ion channel. Other cardiac ion channels tested (i.e., hNav1.5, hCav1.2, and hKCNQ1/min K) were not inhibited at 10 μM.

Compound **1** was well tolerated up to 150 mg/kg, po in a 7-day exploratory toxicology study in rats, as well as up to 100 mg/kg, po bid in a 14-day exploratory toxicology study in mice. No macroscopic pathology, histological lesions, or adverse hematological changes were observed up to the indicated doses. In male rats, there was a dose-proportional increase in exposure ($AUC_{0-8\,h}$) between 3 mg/kg (day 7, C_{max} 4640 nM, T_{max} 1 h, $AUC_{0-8\,h}$ 7160 nM*h) and 150 mg/kg (day 7, C_{max} 39 600 nM, T_{max} 4 h, $AUC_{0-8\,h}$ 210 000 nM*h).

https://doi.org/10.1021/acs.jmedchem.0c02249
J. Med. Chem. 2021, 64, 4891−4902

The exposure also increased in a dose-proportional manner between 3 and 30 mg/kg in female rats, but at 150 mg/kg, the exposure did not increase compared with that at 30 mg/kg. Exposures decreased in both sexes after repeated dosing at 30 mg/kg, as the $AUC_{0-8\,h}$ values after 7-day dosing were 55 and 74% of that obtained after a single dose in male and female rats, respectively. In female mice, repeated dosing at 100 mg/kg (day 14, C_{max} 61 640 nM, T_{max} 1 h, $AUC_{0-8\,h}$ 131 000 nM*h) also reduced the exposure to 33% of that obtained after a single 100 mg/kg dose (day 1, C_{max} 140 000 nM, T_{max} 1 h, $AUC_{0-8\,h}$ 399 000 nM*h). Additional exposure data can be found in Table S1a,b in the Supporting Information.

The reduced exposure after repeated dosing suggests that **1** is enhancing its own rate of clearance, possibly through CYP induction of the rat CYP3A4 orthologue as was observed with human hepatocytes. Induction of metabolism might also explain why the exposure in female rats did not increase at the highest dose. The impact of repeat dosing on exposure should be considered if planning to run repeat dosing experiments. Overall, **1** is considered to have a good safety and tolerability profile supportive of subchronic dosing studies.

To synthesize **1** in sufficient amounts to broadly support its use as a tool, development of scalable routes toward the two coupling partners, thiazole carboxylic acid **23** and diamine **22**, was developed. The optimized synthesis of **1** (Scheme 1) was initiated with a 1,4-conjugated addition of morpholine to nitroolefin **19**, and the corresponding adduct precipitated directly by the addition of 2 M hydrochloric acid. The resulting white solid was isolated via filtration of the reaction mixture affording hydrochloride salt **20**. Attempts to dry hydrochloride **20** in a vacuum oven at 40 °C resulted in the elimination of morpholine affording back nitroolefin **19**; therefore, hydrochloride salt **20** was used directly in the next step. Reduction of the nitro moiety by exposure to zinc in an aqueous ethanolic solution provided racemic diamine **21** in 87% yield. After extensive screening, an enantioselective crystallization resolution method of diamine **21** using *N*-acetyl-L-leucine in a mixture of acetonitrile and water was discovered to afford the *S*-enantiomer **22** in 30% yield and >97% ee. Diamine **22** was subsequently coupled with corresponding carboxylic acid **23** to afford **1** in 16% overall yield, 99% UV purity, and >97% ee.

While a synthesis for intermediate thiazole carboxylic acid **20** was previously reported,[14] an alternative inexpensive, robust, and scalable procedure was developed to support large-scale production of **1** (see Supporting Information Scheme S1 and the associated synthetic procedures).

CONCLUSIONS

In conclusion, herein, we provide molecular pharmacology, ADME/PK, *in vivo* CNS functional activity, and safety data for **1**, which support its utility as a brain-penetrant chemical probe to interrogate the role of the P2X7R in preclinical models of neuroinflammation and CNS diseases. Importantly, a robust synthetic route for this novel small molecule is also described, thus enabling its availability. We believe **1** will be a valuable addition to the existing tools for evaluating the role of the P2X7 receptor in rodent models of CNS diseases.

EXPERIMENTAL SECTION

Materials and Methods. *Drugs.* The synthesis of Lu AF27139, (*S*)-*N*-(2-(4-chlorophenyl)-2-morpholinoethyl)-2-(pyrimidin-2-yl)-4-(trifluoromethyl)thiazole-5-carboxamide **1**, and enantiomer **2** is described below. The final products have >97% enantiomeric excess (ee) as determined by chiral HPLC or supercritical fluid chromatography (SFC). The comparator P2X7R antagonists A-804598 (**6**),[19] CE224,535 (**7**),[20] AZD9056 (**8**),[21] GSK1482160 (**9**),[22,23] AFC5128 (**10**),[24] Actelion compound (**11**),[25] A-740003 (**12**),[26] A-438079 (**13**),[27] Abbott compound (**14**),[28] Pfizer compound (**15**),[29] JNJ-47965567 (**16**),[30] JNJ-42253432 (**17**),[31] and BBG (**18**)[32] were either synthesized as previously described or were readily available from commercial vendors. The ^{1}H NMR and liquid chromatography−mass spectrometry (LC/MS) data for all compounds were consistent with the structure and literature reports. All compounds were greater than 97% pure based on ^{1}H NMR and LC/MS data.

General Methods. Analytical LC−MS and HPLC data were obtained using one of the methods described below.

Method A: System controller, Shimadzu CBM-20A; UV detector, Shimadzu SPD-M20A. Column: C-18 4.6 × 30 mm, 3.5 μm symmetry; column temperature: 60 °C. Mobile phase gradient: solvent A: H_2O with 0.05% v/v trifluoroacetic acid (TFA) and solvent B: Methanol with 0.05% TFA. Flow: 3.0 mL/min

Method B: A Waters Acquity UPLC-MS was used. Column: Acquity UPLC BEH C18 1.7 μm; 2.1 × 50 mm; column temperature: 60 °C; solvent system: A = water/TFA (99.95:0.05) and solvent B = acetonitrile/water/TFA (94.965:5:0.035); Method: Linear gradient elution with A:B = 90:10 to 0:100 in 1.0 min and with a flow rate of 1.2 mL/min.

Method C: HPLC column: Merck LiChroCart 250-4, LiChroSorb RP-8, 5 μm, 250 ×4.6 mm Mobile phase: 20 mM triethylamine/phosphate buffer in water/acetonitrile 50/50, pH = 3.0. Flow: 1.0 mL/min. Temp.: 30 °C.

Method D: Chiral HPLC column: Chiralpak AD-H, 5 my, 250 × 4.6 mm eluent: heptane:ethanol:diethylamine = 90:10:0.1, flow 1.0 mL/min. Temp: 30 °C

^{1}H NMR spectra were recorded at 500 or 600 MHz on Bruker Avance instruments. Tetramethylsilane (TMS) was used as internal reference standard. Chemical shift values are expressed in ppm. The following abbreviations are used for multiplicity of NMR signals: s = singlet, d = doublet, t = triplet, q = quartet, m = multiplet in accordance with the ACS Style Guide.[42]

Synthesis of Lu AF27139. The synthesis of racemic (±)-*N*-(2-(4-chlorophenyl)-2-morpholinoethyl)-2-(pyrimidin-2-yl)-4-(trifluoromethyl)thiazole-5-carboxamide has previously been described.[14] Herein is a convenient enantiomeric synthesis protocol for the preparation of (*S*)-*N*-(2-(4-chlorophenyl)-2-morpholinoethyl)-2-(pyrimidin-2-yl)-4-(trifluoromethyl)thiazole-5-carboxamide (**1**).

*1-Chloro-4-((E)-2-nitro-vinyl)-benzene (**19**).* 4-Chlorobenzaldehyde (200.0 g, 1423 mmol) was dissolved in acetic acid (600.0 mL, 10 550 mmol) and nitromethane (308.2 mL, 5691 mmol) was added, then acetic anhydride (26.85 mL, 284.6 mmol) and ammonium acetate (120.6 g, 1565 mmol) was added. The reaction was heated at reflux for 2 h, then volatiles were removed by evaporation and water was added (400 mL, 20 000 mmol) followed by ethyl acetate (400 mL, 4000 mmol). The solids were filtered and dried to yield the title compound **19** as a brown solid (178.8 g). ^{1}H NMR ($CDCl_3$ 500 MHz): δ ppm 6.88 (d, 1H), 6.48 (d, 1H), 6.47-6.32 (m, 4H). HPLC, t_R (min, Method A) = 1.48.

*4-[1-(4-Chlorophenyl)-2-nitro-ethyl]-morpholine Hydrochloride Salt (**20**).* 1-Chloro-4-((*E*)-2-nitro-vinyl)-benzene **19** (178.8 g, 973.9 mmol) was dissolved in tetrahydrofuran (383.9 mL, 4733 mmol). Morpholine (84.93 mL, 973.9 mmol) was added, and the mixture was stirred for 30 min at RT. Diethyl ether (1329 mL, 12660 mmol) was added followed by 2.0 M HCl in diethyl ether (584.3 mL). Internal temperature increased to 36 °C, and the slurry was stirred for 15 min before being cooled on an ice bath with stirring for 15 min. The solids were filtered and washed with diethyl ether. The resulting title compound **20** was used without further purification in the next step.

*2-(4-Chlorophenyl)-2-morpholin-4-yl-ethylamine (**21**).* 4-[1-(4-Chloro-phenyl)-2-nitro-ethyl]-morpholine, hydrochloride salt **20** (59.0 g, 192 mmol), was suspended in ethanol (680 mL, 12 000 mmol), then 37% aqueous HCl solution (200 mL) was added

https://doi.org/10.1021/acs.jmedchem.0c02249
J. Med. Chem. 2021, 64, 4891−4902

followed by the addition of zinc (42.8 g, 654 mmol) in four portions. The mixture was stirred for 50 min, during which the mixture became a clear almost colorless solution. The volatiles were removed by evaporation, and the aqueous mixture was quenched by pouring into 32% aqueous ammonia solution (400 mL). The organics were extracted with iPrOAc (2 × 100 mL). The combined organic phases were dried (sodium sulfate), filtered, and evaporated to dryness in vacuo using MeCN (3 × 100 mL) to co-evaporate, affording the title compound **21** (45.1 g). ^{1}H NMR ($CDCl_3$ 600 MHz): δ ppm 7.31 (d, 2H), 7.20 (d, 2H), 3.71−3.65 (m, 4H), 3.26 (t, 1H), 3.09−3.04 (m, 1H), 2.96−2.91 (m, 1H), 2.43−2.37 (m, 4H).

(S)-2-(4-Chlorophenyl)-2-morpholin-4-yl-ethylamine-(S)-2-acetylamino-4-methyl-pentanoate. To a solution of 2-(4-chlorophenyl)-2-morpholinoethylamine **21** (106.7 g, 0.443 mol) dissolved in acetonitrile (3005 mL) was added (*S*)-2-acetamido-4-methylpentanoic acid (*N*-acetyl-L-leucine 76.80 g, 0.443 mol), and the mixture was heated to reflux and water (105 mL) was added, giving a clear solution. The heating was stopped, and the solution was allowed to cool slowly to room temperature. At ca. 45 °C, crystallization started and continued over 4 h while cooling slowly to 20 °C. The product was isolated by filtration and washed on the filter with acetonitrile (2 × 100 mL) and dried in vacuo. The solid was resuspended in 240 mL of acetonitrile:water (v/v 96.5:3.5). The slurry was then heated slowly to reflux for 1 h, heating was removed, and stirring was continued while slowly cooling to room temperature (RT). The slurry was stirred for 16 h at RT. The precipitated compound was isolated by filtration, washed on the filter with 2 × 20 mL of acetonitrile:water (v/v 96.5/3.5) and 1 × 30 mL of acetonitrile, and dried. The product was then dried to constant weight in vacuo at 40 °C to yield the title compound as a white solid (55.1 g). ^{1}H NMR ($CDCl_3$ 600 MHz): δ ppm 7.68 (d, 1H), 7.44 (d, 2H), 7.26 (d, 2H), 4.08−4.03 (m, 1H), 3.71−3.68 (m, 1H), 3.58−3.52 (m, 4H), 3.38−3.32 (m, 1H), 2.88−2.83 (m, 1H), 2.40−2.35 (m, 2H), 2.22−2.15 (m, 2H), 1.81 (s, 3H), 1.62−1.55 (m, 1H), 1.50−1.45 (m, 1H), 1.41−1.36 (m, 1H), 0.85 (d, 3H), 0.81 (d, 3H). HPLC t_R (min, Method C) = 2.53.

(S)-2-(4-Chlorophenyl)-2-morpholinoethylamine (22). To a solution of 2-(4-chlorophenyl)-2-morpholinoethylamine (*S*)-2-acetamido-4-methylpentanoate (55.1 g) in iPrOAc/H_2O (400 mL) was added 24% aqueous ammonia. The phases were separated, and the water phase was extracted once more with iPrOAc (50 mL) and the combined organic phases were washed with water (2 ×50 mL), dried over $MgSO_4$, and the solvent was removed in vacuo. NaCl (ca. 20 g) was dissolved in the water phase and then extracted with iPrOAc (3 × 100 mL). The combined organic phases were washed with brine (2 × 50 mL), dried over $MgSO_4$, evaporated, and dried to constant weight to yield the title compound **22** (31.3 g). HPLC t_R (min, Method C) = 2.53, Chiral HPLC t_R (min, Method D) = 14.96

(S)-N-(2-(4-Chlorophenyl)-2-morpholinoethyl)-2-(pyrimidin-2-yl)-4-(trifluoromethyl)thiazole-5-carboxamide (1). (*S*)-2-(4-Chlorophenyl)-2-morpholinoethylamine **22** (31.3 g, 130 mmol) was dissolved in dry THF (700 mL) at RT. 2-(Pyrimidin-2-yl)-4-(trifluoromethyl)thiazole-5-carboxylic acid **23** (39.4 g, 143 mmol, preparation described in supplemental materials) was added followed by triethylamine (54.4 mL, 390 mmol). 2,4,6-Tripropyl-1,3,5,2,4,6-trioxatriphosphinane-2,4,6-trioxide (T3P) (122 mL, 50% solution in ethyl acetate, dissolved in THF 100 mL) was added slowly and resulted quickly in a clear solution. The reaction was stirred at RT for 3 h. To the reaction was added iPrOAc (500 mL), and the organic phase was washed with 0.5 M NaOH (200 mL) and 0.1 M NaOH (200 mL), followed by washing with water (2 × 200 mL). The product was then extracted with 1 M aqueous H_2SO_4 (4 × 200 mL), and the combined water phases were washed with iPrOAc (2 × 200 mL) and was again made basic with 24% aqueous ammonia (strong exotherm, cooled with ice) and extracted with iPrOAc (2 × 400 mL). The combined organic phases were washed with water (1 × 300 mL) and brine (2 × 200 mL), dried over $MgSO_4$, and the solvent was partly removed in vacuo (volume, ca. 400 mL) and heptane (600 mL) was added. The mixture was stirred on a rotary evaporator for 16 h while slowly cooling to room temperature. The reaction was cooled on ice for 30 min, and the product was isolated by filtration, washed with heptane (2 × 50 mL), and dried under vacuum to constant weight to yield the title compound (**1**) (40 g). ^{1}H NMR (DMSO-d_6 600 MHz): δ ppm 9.02 (d, 2H), 8.94 (t, 1H), 7.71 (t, 1H), 7.44 (d, 2H), 7.33 (d, 2H), 3.92−3.86 (m, 1H), 3.67−3.64 (m, 1H), 3.60−3.48 (m, 5H), 2.40−2.30 (m, 4H). LCMS (MH^+): m/z = 498.3, t_R (min, Method B) = 0.49. HPLC t_R (min, Method C) = 5.16. $[\alpha]_D^{20}$ = −34.89 (c = 1% in MeOH). Elemental Analysis (CHN) and KF H_2O: Found C 50.67%, H 3.90%, N 13.76%, KF H_2O < 0.1%. Expected C 50.66%, H 3.85%, N 14.07%.

Stereochemistry Determination of (S)-2-(4-Chlorophenyl)-2-morpholinoethylamine (22). The absolute stereochemistry of chiral amine **22** was determined by XRPD analysis of the corresponding Mosher's amide,[43] which confirmed the *S*-stereochemistry. Stereochemistry assignment of (2*R*)-N-[(2*S*)-2-(4-chlorophenyl)-2-morpholino-ethyl]-3,3,3-trifluoro-2-methoxy-2-phenyl-propanamide was determined from a combination of *R*-factor tests [R_1^+ = 0.0414, R_1^- = 0.0561], Flack parameter [x^+ = −0.02(2), x^- = 1.01(2)], and Bayesian statistics on Bijvoet differences, *p*3(ok), *p*3(twin), and *p*3(wrong) 1.000, 0.000, and 0.000, respectively. Calculation based on 6994 Bijvoet pairs. XRPD was measured on a sample of the batch and gave the same pattern as the one used for the structure determination. This means that the crystal selected for the structure determination is representative of the batch.

P2X7 Inhibition Measured by FLIPR Assays. Human (**NM_002562.5**), mouse (**NM_002562.5**), and rat (**NM_002562.5**) P2X7 receptors were cloned into a pCDNA3.1 vector and stably expressed in HEK 293s cells (passage number <25, ATCC Manassas, VA). The stable cells (15 000/well) were plated in 384-well poly-D-lysine (PDL)-coated black FLIPR plates (Greiner Bio One, Monroe, NC) using 1.5% fetal bovine serum (FBS) (Atlanta Biologicals, Lawrenceville, GA), in Dulbecco's modified Eagle's medium (DMEM) (Gibco—Thermo Fischer Scientific, Waltham MA) 24 h before the assay. The plates were washed 2× with the assay buffer. For the human P2X7R assay, sucrose buffer was used to improve the signal-to-noise ratio (sucrose assay buffer, pH 7.4, 5 mM potassium chloride, 9.6 mM $NaH_2PO_4{\cdot}2H_2O$, 25 mM 2-[4-(2-hydroxyethyl)piperazin-1-yl]ethanesulfonic acid buffer (HEPES), 0.5 mM $CaCl_2$, 5 mM glucose, 280 mM sucrose, and 1.0 mM probenecid (Sigma, St. Louis, MO)), whereas for rat and mouse P2X7R, regular FLIPR buffer was used [Hank's balanced salt solution buffer (HBSS), pH 7.4 1× buffer supplemented with 20 mM HEPES plus 2.5 mM probenecid (Sigma) and 0.05% bovine serum albumin (Sigma)]. After washing, the plates were loaded with 30 μL of Fluo-4 NW in Fluo-4 NW Calcium Assay Kit buffer (Molecular Probes, Eugene, OR) and were incubated at 37 °C for 30 min in a humidified chamber (5% CO_2/95% air) and for 30 min at RT. Mobilization of intracellular Ca^{+2} in response to the various P2X7 antagonists was measured online using the FLIPR Tetra reader. In the assay, baseline fluorescence was measured for 15 s, and then 15 μL of compounds (40 μM) was added and fluorescence was monitored for 3 min for agonist activity. Subsequently, 15 μL of BzATP (hP2X7 1 × 8 μM, rP2X7 1 × 15 μM) was added, and after a 30 min incubation at room temperature, the fluorescence was read for 3 min for IC_{50} determination. Data were analyzed using Lundbeck's LSP curve-fit software, which is similar to Prism nonlinear regression curve-fit analysis.

P2X7R Binding Assays. *In vitro* binding was performed in membranes prepared from HEK293 cells stably transfected with mouse, rat, or human P2X7 using [^{3}H]-A-804598 as the radio-ligand. Binding was performed in assay buffer (50 mM Tris-HCL, 0.1% BSA, pH 7.4) at 4 °C for 1 h in a total volume of 250 μL using either 10 μg of rat P2X7R, 40 μg of human P2X7R, or 60 μg of mouse P2X7R membranes per well. The membranes were prepared using 25 mM Tris-HCl, pH 7.4, 250 mM sucrose, 2.5 mM ethylenediaminetetraacetic acid (EDTA), 2 μg/mL aprotinin, 0.5 μg/mL leupeptin, and 200 nM phenylmethanesulfonyl fluoride (PMSF). Nonspecific binding was defined using 10 μM cold A-804598. K_d was determined by concentration-dependent saturation binding using 10 concentrations of [^{3}H]-A-804598 (0.5−50 nM).

https://doi.org/10.1021/acs.jmedchem.0c02249
J. Med. Chem. 2021, 64, 4891−4902

THP-1 Cell IL-1β Assay. THP-1 cells (passage number <15, ATCC, Manassas, VA) were maintained in growth media (RPMI1640, 10% FBS (Atlanta Biologicals), 100 units/mL penicillin and 100 μg/mL streptomycin (P/S), and 0.05 mM β-mercaptoethanol) (all except FBS from Gibco)) and differentiated with 10 ng/mL of interferon γ (IFN-γ) (R&D Systems, Minneapolis, MN) over 48 h at 37 °C and 5% CO_2. The differentiated cells were removed from the T150 flasks and resuspended in CTL test media (Cellular Technology Limited, OH) containing 1% Glutamax. Cells were primed by adding lipopolysaccharide (LPS) (Sigma) to a final concentration of 100 ng/mL, and then plated into PDL-coated 96-well plates at a density of 10k cells/well. The plates were covered with Breathe-Easier microplate sealing tape and incubated at 37 °C and 5% CO_2 for 3.5 h. Test compounds diluted in CTL test media were added to the cells and incubated for 20 min at 37 °C and 5% CO_2. BzATP was then added to the cells at a final concentration of 1 mM and incubated for an additional 30 min at 37 °C and 5% CO_2. The supernatant from the wells was transferred into a 384-well polypropylene plate. The IL-1β levels in the supernatants were measured using human AlphaLISA IL-1β immunoassay (PerkinElmer) and an Envision microplate reader (PerkinElmer, Waltham, MA).

Rat Primary Microglia Cultures. Female Sprague−Dawley rats (Crl:SD, Charles River, Kingston, NY; E14 timed pregnant at delivery) were singly housed at 20−22 °C on a 12 h dark/light cycle with food and water ad libitum. Primary microglia cultures were prepared from postnatal day 3 (P3).

Microglia were cultured as described.[44] Briefly, the animals were euthanized by CO_2 anesthesia followed by decapitation. The brains were removed, and cortices were dissected out and chopped in ice-cold HBSS (Gibco). The tissue was mechanically triturated by pipette to obtain a single-cell suspension. Cortical suspension from one rat or two mice were plated into a single T150 flask (BD Falcon, Corning, NY) in DMEM-GlutaMax (Gibco) containing 4.5 g/L of D-glucose and supplemented with 10% low endotoxin (0.06 EU/mL) FBS (Atlanta Biologicals) and 1% P/S (Gibco).

Cultures were grown in a humidified incubator at 37 °C under 5% CO_2 for 10−14 days, during which time microglia were harvested by tapping the flasks and collecting microglia floating in the medium. Microglia were pelleted by centrifugation at 1100 rpm (276*g*) on a Beckman Coulter (Brea, CA) Allegra 6 series with a GH-3.8 swing bucket rotor for 5 min, resuspended in DMEM/10%FBS/P/S medium, and plated at an assay-specific density in poly-D-lysine (PDL)-coated plates (BD Falcon). Purity was assessed by labeling with the microglial maker CD11b, which routinely identified >95% of cells as microglia.

Electrophysiology. *Compound Preparation.* A 10 mM stock solution of Lu AF27139 in dimethyl sulfoxide (DMSO) was prepared immediately before use and diluted with extracellular solution buffer to the desired concentrations. Glass vial inserts were filled with 350−400 μL of compound solution and placed into the glass insert base plate for use in the QPatch assay, or in a capillary tube for recording in rat primary microglia.

QPatch DRC in HEK293 Cells Expressing the Rat P2X7R. HEK293 cells stably expressing rat P2X7 were grown in T75 tissue culture flasks to 70−80% confluence. On the day of the experiment, the cells were washed with D-PBS, lifted with 2 mL of Detachin, and centrifuged (250*g*, 2 min). The supernatant was removed, and the cells were washed and resuspended in extracellular solution to achieve a final cell density of ∼3 × 10^6 cells/mL.

QPatch Electrophysiology. Whole-cell patch-clamp experiments were carried out on a QPatch-16 automated electrophysiology platform (Sophion Biosciences, Paramus, NJ). Following establishment of the whole-cell configuration, the cells were held at −60 mV. The extracellular solution contained 140 mM NaCl, 4 mM KCl, 0.1 mM $MgCl_2$, 0.3 mM $CaCl_2$, 10 mM HEPES, and 10 mM glucose at pH 7.4. The intracellular solution contained 140 mM $CsCl_2$, 11 mM EGTA, 2 mM $MgCl_2$, and 10 mM HEPES at pH 7.2. P2X7 currents were elicited with 100 μM BzATP (Sigma). Currents were analyzed using the Sophion QPatch software and exported to Microsoft Excel and GraphPad Prism 6 software (GraphPad Software, Inc) for further analysis.

Electrophysiology Recordings from Rat Primary Microglia. Primary rat microglia were seeded at a density of 300 000/35 mm dish for 24 h. Whole-cell patch-clamp recordings were performed using an EPC9 patch-clamp amplifier and PatchMaster software (HEKA Instruments, Inc., Holliston, MA). The cell's membrane potential was held at −60 mV. External solution contained 140 mM NaCl, 4 mM KCl, 1 mM $MgCl_2$, 1.8 mM $CaCl_2$, 10 mM HEPES, and 10 mM glucose at pH 7.4. The patch solution contained 140 mM $CsCl_2$, 11 mM EGTA, 2 mM $MgCl_2$, and 10 mM HEPES, pH 7.2. Compound **1** was applied by gravity via a capillary tube placed in close proximity to the recording dish. P2X7R currents were elicited by application of 300 μM BzATP for 10 s.

IL-1β Measurements in Mouse and Rat Microglia. The IL-1β assay was conducted 1 day after rat microglia (100 000 cells/well/48 well plate) or mouse microglia (50 000 cells/well/96-well plate) were plated on PDL-coated plates (BD Falcon). The cells were primed with 3 EU/mL LPS (Control Standard Endotoxin, Associates of Cape Cod) for 3.5 h. Vehicle or **1** was added and incubated for an additional 30 min. BzATP was then added to the cells at a final concentration of 1 mM and incubated for an additional 30 min at 37 °C and 5% CO_2. All treatments were added to wells sequentially without any media being removed or changed. Post incubation, the supernatant was collected and analyzed for IL-1β as per the manufacturer's protocol (mouse: N45ZA-1, rat: N45IA-1; MesoScale Discovery, Rockville, MD). IL-1β levels were normalized to total protein as determined using the BCA protein assay kit (Thermo Scientific, Rockford, IL). IC_{50} values were generated using GraphPad Prism 6 software (GraphPad Software, Inc., San Diego, CA). The data were expressed as mean ± standard deviation (SD).

Mouse and Rat Microdialysis. Male Sprague−Dawley rats (Crl:SD, Charles River) (280−350 g) were implanted with a guide cannulas (BrainLink, Groningen, The Netherlands) into the frontal cortex (FC), and an additional cannula for intracerebroventricular (icv) injections was implanted into the lateral cerebral ventricle. Male C57BL (C57BL/6NCrl, Charles River, Kingston, NY) mice (18−25 g) were implanted with guide cannulas (BrainLink, Groningen, The Netherlands) into the frontal cortex (FC) and an additional cannula for intracerebroventricular (icv) injections into the lateral cerebral ventricle (N = 6−7). Both implantations were completed in one surgery. Seven days after surgery, microdialysis probes (2 mm polyethylene membrane), 3000 kDa molecular weight cutoff (BrainLink, Groningen, The Netherlands), were inserted via the guide cannula into the FC. The animals were then placed in plastic observation cages and connected to a two-channel swivel. The input of the dialysis probe was connected to a syringe pump, which delivered artificial cerebrospinal fluid (CSF, perfusion fluid CNS, M Dialysis AB, Stockholm, Sweden) with 0.15% human serum albumin to the probe at a rate of 0.7 μL/min overnight. The output from the swivel was attached to a peristaltic pump (EICOM USA, San Diego, CA) and a refrigerated fraction collector using a "push−pull" microdialysis method. After overnight perfusion, samples were collected every 60 min. LPS (rat: 3 μg/5 μL; mouse: 0.1 μg/3 μL) was injected icv 1 h prior to oral administration of Lu AF27139 or vehicle (20% 2-hydroxypropyl-β-cyclodextrin). BzATP (rat: 50 μg/5 μL; mouse: 5 μg/3 μL) was given icv 1 h after administration of **1** or vehicle. During microdialysis sampling, the conscious, unrestrained animals were housed in the animal containment system with free access to food and water. Microdialysis samples were kept at −80 °C until IL-1β analyses. IL-1β in the microdialysate samples was analyzed using custom and standard V-PLEX assays from MesoScale Discovery (Rockville, MD). The lower limit of detection was 2 pg/mL for IL-1β. Graphical and statistical analysis was done using GraphPad Prism software (version 5.01). An area under the curve (AUC) value was calculated from the baseline for each animal from time 0 to 5 h. A one-way analysis of variance (ANOVA) with Dunnett's multiple comparison test was used to determine significance between treatment groups.

https://doi.org/10.1021/acs.jmedchem.0c02249
J. Med. Chem. 2021, 64, 4891−4902

Ethical Statement. All animal procedures were conducted in accordance with the Guide for Care and Use of Laboratory Animals[45] and with the approval of the Institutional Animal Care and Use Committees at Lundbeck Research USA.

Experimental Animals. Unless noted otherwise, all *in vivo* experiments were conducted with male Sprague−Dawley (Crl:SD, Charles River) rats weighing 150−200 g. The animals were subjected to an acclimation period of 7 days prior to using for experiments and were maintained under standard husbandry conditions (22 °C, 35−50% relative humidity, 12 h light/dark cycle), with unrestricted access to standard rat chow and drinking water.

Formulation and Dosing Compound 1. Unless mentioned otherwise, for *in vivo* experiments, **1** was formulated as a solution or fine suspension in 20% hydroxypropyl-β-cyclodextrin and administered via oral gavage at a volume of 5 or 10 mL/kg.

■ ASSOCIATED CONTENT

Supporting Information

The Supporting Information is available free of charge at https://pubs.acs.org/doi/10.1021/acs.jmedchem.0c02249.

Scheme S1; synthesis of intermediate **20** and associated detailed synthetic methods; liver microsomal stability assay; hepatocyte stability assay; MDCK-MDR1 permeability assay; compound **1** exposure and fraction unbound in plasma, brain, and spinal cord; LC−MS/MS method for analysis of compound **1** from exposure studies; Rat PK methods; *in vivo* exploratory toxicology study methods; and Tables S1a and S1b with rat and mouse toxicokinetic exposure data (PDF)

Structure smiles (CSV)

■ AUTHOR INFORMATION

Corresponding Author

Allen T. Hopper − *Neuroinflammation Disease Biology Unit Lundbeck Research USA, Paramus, New Jersey 07652, United States;* orcid.org/0000-0001-8797-7882; Email: athopper@aol.com

Authors

Martin Juhl − *Process Research Lundbeck A/S, 2500 Valby, Denmark*

Jorrit Hornberg − *Toxicology Research Lundbeck A/S, 2500 Valby, Denmark*

Lassina Badolo − *Chemistry and DMPK Lundbeck A/S, 2500 Valby, Denmark*

John Paul Kilburn − *Chemistry and DMPK Lundbeck A/S, 2500 Valby, Denmark*

Annemette Thougaard − *Toxicology Research Lundbeck A/S, 2500 Valby, Denmark*

Gennady Smagin − *Neuroinflammation Disease Biology Unit Lundbeck Research USA, Paramus, New Jersey 07652, United States*

Dekun Song − *Neuroinflammation Disease Biology Unit Lundbeck Research USA, Paramus, New Jersey 07652, United States*

Londye Calice − *Neuroinflammation Disease Biology Unit Lundbeck Research USA, Paramus, New Jersey 07652, United States*

Veena Menon − *Neuroinflammation Disease Biology Unit Lundbeck Research USA, Paramus, New Jersey 07652, United States*

Elena Dale − *Neuroinflammation Disease Biology Unit Lundbeck Research USA, Paramus, New Jersey 07652, United States*

Hong Zhang − *Neuroinflammation Disease Biology Unit Lundbeck Research USA, Paramus, New Jersey 07652, United States*

Manuel Cajina − *Neuroinflammation Disease Biology Unit Lundbeck Research USA, Paramus, New Jersey 07652, United States*

Megan E. Nattini − *Neuroinflammation Disease Biology Unit Lundbeck Research USA, Paramus, New Jersey 07652, United States*

Adarsh Gandhi − *Neuroinflammation Disease Biology Unit Lundbeck Research USA, Paramus, New Jersey 07652, United States*

Michel Grenon − *Neuroinflammation Disease Biology Unit Lundbeck Research USA, Paramus, New Jersey 07652, United States*

Ken Jones − *Neuroinflammation Disease Biology Unit Lundbeck Research USA, Paramus, New Jersey 07652, United States*

Tanzilya Khayrullina − *Neuroinflammation Disease Biology Unit Lundbeck Research USA, Paramus, New Jersey 07652, United States*

Gamini Chandrasena − *Neuroinflammation Disease Biology Unit Lundbeck Research USA, Paramus, New Jersey 07652, United States*

Christian Thomsen − *Neuroinflammation Disease Biology Unit Lundbeck Research USA, Paramus, New Jersey 07652, United States*

Stevin H. Zorn − *Neuroinflammation Disease Biology Unit Lundbeck Research USA, Paramus, New Jersey 07652, United States*

Robb Brodbeck − *Neuroinflammation Disease Biology Unit Lundbeck Research USA, Paramus, New Jersey 07652, United States*

Suresh Babu Poda − *Neuroinflammation Disease Biology Unit Lundbeck Research USA, Paramus, New Jersey 07652, United States*

Roland Staal − *Neuroinflammation Disease Biology Unit Lundbeck Research USA, Paramus, New Jersey 07652, United States*

Thomas Möller − *Neuroinflammation Disease Biology Unit Lundbeck Research USA, Paramus, New Jersey 07652, United States*

Complete contact information is available at: https://pubs.acs.org/10.1021/acs.jmedchem.0c02249

Author Contributions

A.T.H., M.J., M.G., and P.K. supported Lu AF27139 identification, synthesis, and project leadership. G.S. and D.S. supported microdialysis studies. J.H., A.T., M.C., and G.C. supported safety evaluation and toxicokinetics. L.B., M.C., A.G., M.E.N., and G.C. supported ADME/PK. R.S., L.D., V.M., E.D., H.Z., C.T., S.H.Z., K.J., T.K., R.M.B., S.B.P., and T.M. supported *in vitro* molecular pharmacological characterization. These authors contributed equally.

Funding

This research was completely funded by Lundbeck Research USA or H. Lundbeck A/S.

Notes

The authors declare no competing financial interest.

■ ACKNOWLEDGMENTS

The authors kindly acknowledge and thank the Lundbeck organization for their complete support, including financial support, for this project. They also acknowledge Dario Dollar and Benny Bang-Anderson for their input, challenge, and feedback in support of this work.

■ ABBREVIATIONS

AD, Alzheimer's disease; ATP, adenosine triphosphate; BzATP, 2′(3′)-*O*-(benzoylbenzoyl)adenosine-5′-triphosphate; Clint, intrinsic clearance; CSF, cerebrospinal fluid; C_u, concentration unbound; DMEM, Dulbecco's modified Eagle's medium; D-PBS, Dulbecco's phosphate-buffered saline; FBS, fetal bovine serum; FC, frontal cortex; FLIPR, fluorescent imaging plate reader; f_u, fraction unbound; HBSS, Hank's balanced salt solution buffer; HEPES, 2-[4-(2-hydroxyethyl)-piperazin-1-yl]ethanesulfonic acid buffer; ICV, intracerebroventricular; LBF, liver blood flow; LPS, lipopolysaccharide; MDD, major depressive disorder; MS, multiple sclerosis; NPP, neuropathic pain; PMSF, phenylmethanesulfonyl fluoride; P2X7R, P2X purinoceptor 7; P/S, penicillin−streptomycin

■ REFERENCES

(1) Bartlett, R.; Stokes, L.; Sluyter, R. The P2X7 receptor channel: recent developments and the use of P2X7 antagonists in models of disease. *Pharmacol. Rev.* **2014**, *66*, 638−675.

(2) Sperlágh, B.; Vizi, E. S.; Wirkner, K.; Illes, P. P2X7 receptors in the nervous system. *Prog. Neurobiol.* **2006**, *78*, 327−346.

(3) Solle, M.; Labasi, J.; Perregaux, D. G.; Stam, E.; Petrushova, N.; Koller, B. H.; Griffiths, R. J.; Gabel, C. A. Altered cytokine production in mice lacking P2X7 receptors. *J. Biol. Chem.* **2001**, *276*, 125−132.

(4) Burnstock, G. P2X ion channel receptors and inflammation. *Purinergic Signalling* **2016**, *12*, 59−67.

(5) Sperlágh, B.; Illes, P. P2X7 receptor: an emerging target in central nervous system diseases. *Trends Pharmacol. Sci.* **2014**, *35*, 537−547.

(6) Andrejew, R.; Oliveira-Giacomelli, A.; Ribeiro, D. E.; Glaser, T.; Arnaud-Sampaio, V. F.; Lameu, C.; Ulrich, H. The P2X7 receptor: central hub of brain diseases. *Front. Mol. Neurosci.* **2020**, *13*, No. 124.

(7) Bhattacharya, A. Recent advances in CNS P2x7 physiology and pharmacology: focus on neuropsychiatric disorders. *Front. Pharmacol.* **2018**, *9*, No. 30.

(8) Calzaferri, F.; Ruiz-Ruiz, C.; de Diego, A. M. G.; de Pascual, R.; Mendez-Lopez, I.; Cano-Abad, M. F.; Maneu, V.; de los Rios, C.; Gandia, L.; Garcia, A. G. The purinergic P2X7 receptor as a potential drug target to combat neuroinflammation in neurodegenerative diseases. *Med. Res. Rev.* **2020**, *40*, 2427−2465.

(9) Chessell, I. P.; Hatcher, J. P.; Bountra, C.; Michel, A. D.; Hughes, J. P.; Green, P.; Egerton, J.; Murfin, M.; Richardson, J.; Peck, W. L.; Grahames, C. B. A.; Casula, M. A.; Yiangou, Y.; Birch, R.; Anand, P.; Buell, G. N. Disruption of the P2X7 purinoceptor gene abolishes chronic inflammatory and neuropathic pain. *Pain* **2005**, *114*, 386−396.

(10) Bhattacharya, A.; Derecki, N. C.; Lovenberg, T. W.; Drevets, W. C. Role of neuro-immunological factors in the pathophysiology of mood disorders. *Psychopharmacology* **2016**, *233*, 1623−1636.

(11) Bhattacharya, A.; Lord, B.; Grigoleit, J.-S.; He, Y.; Fraser, I.; Campbell, S. N.; Taylor, N.; Aluisio, L.; O'Connor, J. C.; Papp, M.; Chrovian, C.; Carruthers, N.; Lovenberg, T. W.; Letavic, M. A. Neuropsychopharmacology of JNJ-55308942: evaluation of a clinical candidate targeting P2X7 ion channels in animal models of neuroinflammation and anhedonia. *Neuropsychopharmacology* **2018**, *43*, 2586−2596.

(12) Chrovian, C. C.; Rech, J. C.; Bhattacharya, A.; Letavic, M. A. P2X7 antagonists as potential therapeutic agents for the treatment of CNS disorders. *Prog. Med. Chem.* **2014**, *53*, 65−100.

(13) Swanson, D. M.; Savall, B. M.; Coe, K. J.; Schoetens, F.; Koudriakova, T.; Skaptason, J.; Wall, J.; Rech, J.; Deng, X.; De Angelis, M.; Everson, A.; Lord, B.; Wang, Q.; Ao, H.; Scott, B.; Sepassi, K.; Lovenberg, T. W.; Carruthers, N. I.; Bhattacharya, A.; Letavic, M. A. Identification of (R)-(2-Chloro-3-(trifluoromethyl)-phenyl)(1-(5-fluoropyridin-2-yl)-4-methyl-6,7-dihydro-1H-imidazo-[4,5-c]pyridin-5(4H)-yl)methanone (JNJ 54166060), a Small Molecule Antagonist of the P2X7 receptor. *J. Med. Chem.* **2016**, *59*, 8535−8548.

(14) Li, H.; Yuan, J.; Bakthavatchalam, R.; Hodgetts, K. J.; Capitosti, S. M.; Mao, J.; Wustrow, D. J.; Guo, Q. Preparation of 5-membered Heterocyclic Amides and Related Compounds as Specific Receptor Activity Modulators. WO Patent WO20090124822009.

(15) Kilburn, J. P.; Hopper, A. T.; Juhl, M. Enantiomeric Synthesis of (S)-N-[2-(4-Chlorophenyl)-2-morpholinoethyl]-2-(pyrimidin-2-yl)-4-(trifluoromethyl)thiazole-5-carboxamide as a Potent P2X7 Purinergic Receptor Inhibitor. WO Patent WO20170768252017.

(16) Rech, J. C.; Bhattacharya, A.; Letavic, M. A.; Savall, B. M. The evolution of P2X7 antagonists with a focus on CNS indications. *Bioorg. Med. Chem. Lett.* **2016**, *26*, 3838−3845.

(17) Letavic, M. A.; Savall, B. M.; Allison, B. D.; Aluisio, L.; Andres, J. I.; De Angelis, M.; Ao, H.; Beauchamp, D. A.; Bonaventure, P.; Bryant, S.; Carruthers, N. I.; Ceusters, M.; Coe, K. J.; Dvorak, C. A.; Fraser, I. C.; Gelin, C. F.; Koudriakova, T.; Liang, J.; Lord, B.; Lovenberg, T. W.; Otieno, M. A.; Schoetens, F.; Swanson, D. M.; Wang, Q.; Wickenden, A. D.; Bhattacharya, A. 4-Methyl-6,7-dihydro-4H-triazolo[4,5-c]pyridine-Based P2X7 Receptor Antagonists: Optimization of Pharmacokinetic Properties Leading to the Identification of a Clinical Candidate. *J. Med. Chem.* **2017**, *60*, 4559−4572.

(18) Ameriks, M. K.; Ao, H.; Carruthers, N. I.; Lord, B.; Ravula, S.; Rech, J. C.; Savall, B. M.; Wall, J. L.; Wang, Q.; Bhattacharya, A.; Letavic, M. A. Preclinical characterization of substituted 6,7-dihydro-[1,2,4]triazolo[4,3-a]pyrazin-8(5H)-one P2X7 receptor antagonists. *Bioorg. Med. Chem. Lett.* **2016**, *26*, 257−261.

(19) Donnelly-Roberts, D. L.; Namovic, M. T.; Surber, B.; Vaidyanathan, S. X.; Perez-Medrano, A.; Wang, Y.; Carroll, W. A.; Jarvis, M. F. [3H]A-804598 ([3H]2-cyano-1-[(1S)-1-phenylethyl]-3-quinolin-5-ylguanidine) is a novel, potent, and selective antagonist radioligand for P2X7 receptors. *Neuropharmacology* **2008**, *56*, 223−229.

(20) Duplantier, A. J.; Dombroski, M. A.; Subramanyam, C.; Beaulieu, A. M.; Chang, S.-P.; Gabel, C. A.; Jordan, C.; Kalgutkar, A. S.; Kraus, K. G.; Labasi, J. M.; Mussari, C.; Perregaux, D. G.; Shepard, R.; Taylor, T. J.; Trevena, K. A.; Whitney-Pickett, C.; Yoon, K. Optimization of the physicochemical and pharmacokinetic attributes in a 6-azauracil series of P2X7 receptor antagonists leading to the discovery of the clinical candidate CE-224,535. *Bioorg. Med. Chem. Lett.* **2011**, *21*, 3708−3711.

(21) Keystone, E. C.; Wang, M. M.; Layton, M.; Hollis, S.; McInnes, I. B. Clinical evaluation of the efficacy of the P2X7 purinergic receptor antagonist AZD9056 on the signs and symptoms of rheumatoid arthritis in patients with active disease despite treatment with methotrexate or sulphasalazine. *Ann. Rheum. Dis.* **2012**, *71*, 1630−1635.

(22) Ali, Z.; Laurijssens, B.; Ostenfeld, T.; McHugh, S.; Stylianou, A.; Scott-Stevens, P.; Hosking, L.; Dewit, O.; Richardson, J. C.; Chen, C. Pharmacokinetic and pharmacodynamic profiling of a P2X7 receptor allosteric modulator GSK1482160 in healthy human subjects. *Br. J. Clin. Pharmacol.* **2013**, *75*, 197−207.

(23) Abdi, M. H.; Beswick, P. J.; Billinton, A.; Chambers, L. J.; Charlton, A.; Collins, S. D.; Collis, K. L.; Dean, D. K.; Fonfria, E.; Gleave, R. J.; Lejeune, C. L.; Livermore, D. G.; Medhurst, S. J.; Michel, A. D.; Moses, A. P.; Page, L.; Patel, S.; Roman, S. A.; Senger, S.; Slingsby, B.; Steadman, J. G. A.; Stevens, A. J.; Walter, D. S. Discovery and structure-activity relationships of a series of pyroglutamic acid amide antagonists of the P2X7 receptor. *Bioorg. Med. Chem. Lett.* **2010**, *20*, 5080−5084.

https://doi.org/10.1021/acs.jmedchem.0c02249
J. Med. Chem. 2021, 64, 4891−4902

(24) Boes, M. Preparation of Indole-3-Carboxamide or Azaindole-3-Carboxamide Compounds as P2x7R Antagonists for Treating Multiple Sclerosis. U.S. Patent US201301970462013.
(25) Hilpert, K.; Hubler, F.; Kimmerlin, T.; Murphy, M.; Renneberg, D.; Stamm, S. Preparation of Heterocyclic Amide Derivatives as P2X7 Receptor Antagonists. WO Patent WO20130145872013.
(26) Honore, P.; Donnelly-Roberts, D.; Namovic, M. T.; Hsieh, G.; Zhu, C. Z.; Mikusa, J. P.; Hernandez, G.; Zhong, C.; Gauvin, D. M.; Chandran, P.; Harris, R.; Medrano, A. P.; Carroll, W.; Marsh, K.; Sullivan, J. P.; Faltynek, C. R.; Jarvis, M. F. A-740003 [N-(1-{[(cyanoimino)(5-quinolinylamino) methyl]amino}-2,2-dimethylpropyl)-2-(3,4-dimethoxyphenyl)acetamide], a novel and selective P2X7 receptor antagonist, dose-dependently reduces neuropathic pain in the rat. *J. Pharmacol. Exp. Ther.* **2006**, *319*, 1376−1385.
(27) Nelson, D. W.; Gregg, R. J.; Kort, M. E.; Perez-Medrano, A.; Voight, E. A.; Wang, Y.; Grayson, G.; Namovic, M. T.; Donnelly-Roberts, D. L.; Niforatos, W.; Honore, P.; Jarvis, M. F.; Faltynek, C. R.; Carroll, W. A. Structure-Activity Relationship Studies on a Series of Novel, Substituted 1-Benzyl-5-phenyltetrazole P2X7 Antagonists. *J. Med. Chem.* **2006**, *49*, 3659−3666.
(28) Able, S. L.; Fish, R. L.; Bye, H.; Booth, L.; Logan, Y. R.; Nathaniel, C.; Hayter, P.; Katugampola, S. D. Receptor localization, native tissue binding and ex vivo occupancy for centrally penetrant P2X7 antagonists in the rat. *Br. J. Pharmacol.* **2011**, *162*, 405−414.
(29) Chen, X.; Pierce, B.; Naing, W.; Grapperhaus, M. L.; Phillion, D. P. Discovery of 2-chloro-N-((4,4-difluoro-1-hydroxycyclohexyl)-methyl)-5-(5-fluoropyrimidin-2-yl)benzamide as a potent and CNS penetrable P2X7 receptor antagonist. *Bioorg. Med. Chem. Lett.* **2010**, *20*, 3107−3111.
(30) Bhattacharya, A.; Wang, Q.; Ao, H.; Shoblock, J. R.; Lord, B.; Aluisio, L.; Fraser, I.; Nepomuceno, D.; Neff, R. A.; Welty, N.; Lovenberg, T. W.; Bonaventure, P.; Wickenden, A. D.; Letavic, M. A. Pharmacological characterization of a novel centrally permeable P2X7 receptor antagonist: JNJ-47965567. *Br. J. Pharmacol.* **2013**, *170*, 624−640.
(31) Lord, B.; Aluisio, L.; Shoblock, J. R.; Neff, R. A.; Varlinskaya, E. I.; Ceusters, M.; Lovenberg, T. W.; Carruthers, N.; Bonaventure, P.; Letavic, M. A.; Deak, T.; Drinkenburg, W.; Bhattacharya, A. Pharmacology of a novel central nervous system-penetrant P2X7 antagonist JNJ-42253432. *J. Pharmacol. Exp. Ther.* **2014**, *351*, 628−641.
(32) Jiang, L.-H.; Mackenzie, A. B.; North, R. A.; Surprenant, A. Brilliant blue G selectively blocks ATP-gated rat P2X7 receptors. *Mol. Pharmacol.* **2000**, *58*, 82−88.
(33) Young, M. T.; Pelegrin, P.; Surprenant, A. Amino acid residues in the P2X7 receptor that mediate differential sensitivity to ATP and BzATP. *Mol. Pharmacol.* **2007**, *71*, 92−100.
(34) Pelegrin, P.; Surprenant, A. Pannexin-1 mediates large pore formation and interleukin-1β release by the ATP-gated P2X7 receptor. *EMBO J.* **2006**, *25*, 5071−5082.
(35) Liu, X.; Vilenski, O.; Kwan, J.; Apparsundaram, S.; Weikert, R. Unbound brain concentration determines receptor occupancy: a correlation of drug concentration and brain serotonin and dopamine reuptake transporter occupancy for eighteen compounds in rats. *Drug Metab. Dispos.* **2009**, *37*, 1548−1556.
(36) Weinstein, J. R.; Swarts, S.; Bishop, C.; Hanisch, U.-K.; Möller, T. Lipopolysaccharide is a frequent and significant contaminant in microglia-activating factors. *Glia* **2008**, *56*, 16−26.
(37) Hornberg, J. J.; Laursen, M.; Brenden, N.; Persson, M.; Thougaard, A. V.; Toft, D. B.; Mow, T. Exploratory toxicology as an integrated part of drug discovery. Part I: Why and how. *Drug Discovery Today* **2014**, *19*, 1131−1136.
(38) Hornberg, J. J.; Laursen, M.; Brenden, N.; Persson, M.; Thougaard, A. V.; Toft, D. B.; Mow, T. Exploratory toxicology as an integrated part of drug discovery. Part II: Screening strategies. *Drug Discovery Today* **2014**, *19*, 1137−1144.
(39) Flückiger-Isler, S.; Kamber, M. Direct comparison of the Ames microplate format (MPF) test in liquid medium with the standard Ames pre-incubation assay on agar plates by use of equivocal to weakly positive test compounds. *Mutat. Res., Genet. Toxicol. Environ. Mutagen.* **2012**, *747*, 36−45.
(40) Thougaard, A. V.; Christiansen, J.; Mow, T.; Hornberg, J. J. Validation of a high throughput flow cytometric *in vitro* micronucleus assay including assessment of metabolic activation in TK6 cells. *Environ. Mol. Mutagen.* **2014**, *55*, 704−718.
(41) Walmsley, R. M.; Tate, M. The GADD45a-GFP GreenScreen HC assay. *Methods Mol. Biol.* **2012**, *817*, 231−250.
(42) Nadziejka, D. E. *The ACS Style Guide: A Manual for Authors and Editors*, 2nd ed.; ACS Publications, 1997.
(43) Roszkowski, P.; Wojtasiewicz, K.; Leniewski, A.; Maurin, J. K.; Lis, T.; Czarnocki, Z. Enantioselective synthesis of 1-substituted tetrahydro-β-carboline derivatives via asymmetric transfer hydrogenation. *J. Mol. Catal. A: Chem.* **2005**, *232*, 143−149.
(44) Möller, T.; Hanisch, U.-K.; Ransom, B. R. Thrombin-induced activation of cultured rodent microglia. *J. Neurochem.* **2000**, *75*, 1539−1547.
(45) Bayne, K. Revised Guide for the Care and Use of Laboratory Animals available. American Physiological Society. *Physiologist* **1996**, *39*, 208−211.

https://doi.org/10.1021/acs.jmedchem.0c02249
J. Med. Chem. 2021, 64, 4891−4902